ELSEVIER

Polymer 41 (2000) 1183–1191

polymer

High pressure NMR study of chain dynamics in the orthorhombic phase of polyethylene

M. de Langen*, H. Luigjes, K.O. Prins

Van der Waals–Zeeman Institute, University of Amsterdam, Valckenierstraat 65, 1018XE Amsterdam, The Netherlands

Received 16 July 1998; received in revised form 25 January 1999; accepted 18 March 1999

Abstract

At normal conditions crystalline polyethylene (PE) has an orthorhombic structure, whereas at high pressure (above 3200 bar) a phase with a hexagonal structure occurs. We investigate the effect of high pressure (up to about 5000 bar) on the chain motion in PE in the orthorhombic structure and in the vicinity of the transformation to the hexagonal phase. From proton and deuteron NMR spectra and spin–lattice relaxation rates we conclude that, apart from high-frequency mobility at defects, the rigid orthorhombic structure only allows small-angle reorientation of the CH_2 groups on a time scale of the order of 10^{-7} s. The application of high pressure results in a considerable reduction of the amplitude of this motion. The degree of crystallinity is found to increase spectacularly by solidification from the hexagonal phase.

Keywords: Polyethylene; NMR; High pressure

1. Introduction

Experiments on polyethylene using wide line NMR were performed for the first time in 1950 [1]. Since then there have been several NMR studies on the behaviour of the PE molecules in the orthorhombic phase [2–10] and on the melting transition [11,12] for the conventionally crystallized material [13-15] high pressure or solution crystallized material [16–18] (extended chain), and oriented material [9,19,20]. Most of these studies have been performed at ambient pressure only. To investigate polyethylene at high pressure other techniques such as DTA/DSC, X-ray experiments and optical microscopy have been used. Although these techniques can provide very useful information on crystal structure and the position of phase transitions, it is also desirable to perform NMR at high pressure in order to study the chain dynamics under these extreme conditions. This has become possible through the development of the new high pressure NMR equipment published earlier [21].

In this paper we will focus on the orthorhombic phase region of the phase diagram. NMR experiments performed in this phase both at ambient pressure and at high pressure will be presented. The results of these experiments will be discussed in order to get a proper view of what information on the structure and dynamics of PE in the orthorhombic phase region can be obtained.

1.1. Amorphous PE

In the present work, no specific experiments have been performed on the amorphous part of the sample. We note here that the behaviour of amorphous PE has been studied in detail by Hentschel et al. [8,10,13,14] at ambient pressure from low temperature to close to the melting point. A high pressure study has been performed by Kulik et al. [15] for relatively low temperature values (203 to 383 K). Both studies used special pulse sequences to study the amorphous part of the sample exclusively. Some conclusions of these studies are the following. At low temperature the chain motion in the amorphous part of PE is highly restricted. At about 200 K the only observed motion is small angle rotational diffusion. At higher temperature, reorientational jumps between different chain conformations occur on a time-scale of about 5×10^{-6} s. Above 300 K the conformational transitions become less discrete, such that the motion can be characterized as quasi-isotropic diffusion. In the spectrum this is visible as a single structureless line. At increasing pressure, the orientational correlation time shows a gradual increase. The application of 1 kbar of hydrostatic pressure produces an increase of the correlation times corresponding to a decrease of temperature of about 15 K.

* Corresponding author. Tel.: +31-205 256334; fax: +31-205 255788.
E-mail address: langen@phys.uva.nl (M. de Langen)

0032-3861/00/$ - see front matter
PII: S0032-3861(99)00249-9

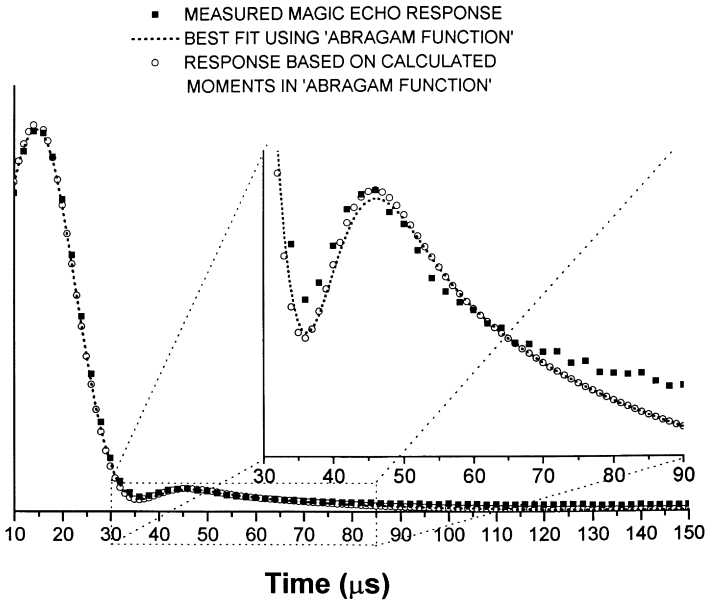

Fig. 1. Approximations using 'Abragam-functions' to the magic echo response observed at 293 K and 1 bar on UHMWPE (Hostalen GUR-403). The inset shows a blow-up of the oscillating region, where the differences between both calculated responses and the observed one are most pronounced.

1.2. NMR spectra and relaxation times

A description of the NMR apparatus and the materials used, has been given in the preceding paper [22]. NMR line shapes can be obtained, in principle, by Fourier transformation of Free Induction Decays (FID) after a $\pi/2$ pulse. In order to overcome receiver dead time limitations our deuteron NMR spectra have been obtained using the quadrupole echo technique [23,24], basically by applying a $(\pi/2)_x - t_1 - (\pi/2)_y - t_1$-acquisition sequence. Because of the limited power levels allowed in the high-pressure probe, we have to compensate for errors introduced in the excitation of the complete spectrum. Therefore, the $\pi/2$ pulses in the sequence have been replaced by 5-fold composite pulses [25,26]. All the experimental ^{2}H NMR spectra presented in the following have been obtained from a quadrupole echo sequence using an inter-pulse spacing t_1 of 40 μs.

Proton NMR spectra are obtained using the "magic-echo" sequence, developed by Rhim et al. [27]. We used their simple pulse sequence consisting of a $[\pi|_x, \pi|_{-x}]^n$ pulse block immediately followed by a $\pi/2|_y$ pulse, resulting in an echo after the last pulse, allowing us to obtain the full spectrum.

Deuteron spin–lattice relaxation has been investigated using a saturation pulse sequence consisting of twenty $\pi/2$ pulses, which after a variable time delay is followed by a quadrupole echo sequence, allowing the separate detection of the relaxation rates in the crystalline and amorphous components via the spectrum. Since spin-diffusion between the protons in these components is fast on the time scale of spin–lattice relaxation, such a distinction cannot be made for the protons. For the measurement of the proton spin–lattice relaxation we therefore do not attempt to observe the complete FID. Instead, we monitor the magnetization after a saturation sequence by a single $\pi/2$ pulse. In the measurement of the rotating frame relaxation times we use a $\pi/2$ pulse followed by a $\pi/2$-phase shifted lock pulse of variable length up to 150 ms. The spin-locking field strength corresponds to about $\nu_1 = 100$ kHz. In our high-pressure probe we did not succeed in generating magic echoes after a locking pulse. By not using echoes in the measurement of rotating frame relaxation we may not see the full contribution of the crystalline part when spin diffusion is not strong enough to make all relaxation times appear equal. However, in high crystallinity material we expect to observe mainly the rotating frame relaxation of the crystalline part.

2. Results and discussion

2.1. Proton NMR spectra

Fig. 1 shows a characteristic time domain response to a magic echo pulse sequence. This signal was obtained at 293 K and 1 bar on a sample of Hostalen GUR 403, crystallized at high pressure in order to obtain highly crystalline extended chain material. The signal clearly consists of a fast decaying part and a smaller slowly decaying part superimposed on each other. Several of our experiments as well as experiments by others [2] have shown that the fast component, which clearly results from the more rigid parts of the sample, originates from crystalline PE. The slower component represents the mobile fraction of the sample. A number of authors also report on an intermediate part [3], which is also observed in some of our experiments. Since our study focusses on the crystalline part of the sample, we will in the

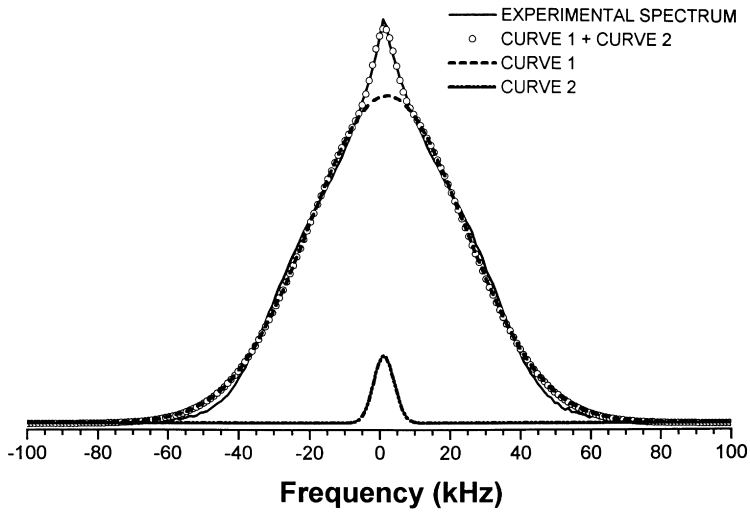

Fig. 2. ^{1}H-NMR spectrum of PE (Hostalen GUR-403) at room temperature and ambient pressure.

following call the complete mobile fraction, including both the amorphous and intermediate parts, the amorphous part of the sample.

The NMR spectrum shown in Fig. 2 was obtained after Fourier transformation of the echo shown in Fig. 1. The crystalline and amorphous parts show up in this spectrum as a broad crystalline component and a narrower amorphous component, respectively. As a guide to the eye this spectrum was approximated by two gaussian functions. Notice that, especially near the wings of the spectra, deviations from a gaussian line shape occur.

For ^{1}H NMR ($I = (1/2)$) the line shape is determined by the magnetic dipole–dipole interactions between all protons in the sample. It is well known [28] that a calculation of the second and fourth moments of the ^{1}H NMR line shape is possible, when the positions of the protons in the crystal structure are known. We have calculated the second and fourth moments of ^{1}H NMR line shape using the information on the orthorhombic crystal structure as presented above and using the lattice parameters ($a = 7.40$ Å, $b = 4.93$ Å, $c = 2.51$ Å) that are known from X-ray measurements [29] at room temperature and ambient pressure. These lattice parameters change somewhat with temperature and pressure, especially on approaching the phase transition. The calculation has been performed using a computer program that was fed all information on the rigid crystal structure. For simplicity only hydrogen atoms within a box with dimensions of about 40 Å around the central atom were considered. Since calculations using a box of twice that size have shown to give an extra contribution to the second moment in the order of only 0.1%, this gives sufficient accuracy. It should be noted here that the calculation of the moments for each of the two hydrogens on each carbon results in slightly different values because these sites are inequivalent in the crystal structure. For a polycrystalline sample the respective second moments are: 1.93×10^{10} rad^2 s^{-2} and 1.85×10^{10} rad^2 s^{-2}. We find for the fourth moments the values 8.89×10^{20} rad^4 s^{-4} and 8.28×10^{20} rad^4 s^{-4}, respectively. These values agree within a few percent with calculated values reported in the literature [16,20].

In order to relate the results of the above calculations to the experimental data, it is convenient to use an analytical representation of the time domain signal, proposed by Abragam [28], which has proven to describe the time domain signal in many rigid lattice solids. The function we have used is

$$G(t) = p_1\left[\frac{\sin bt}{bt}\mathrm{e}^{-\frac{1}{2}a^2t^2}\right] + p_2[\mathrm{e}^{-ct}], \quad (1)$$

in which the first term, representing the crystalline fraction $p_1 (= 0.87$ in this case), is the so-called Abragam function and the second term, representing the amorphous fraction $p_2 (= 0.13)$, is assumed to be exponential. The relation between the quantities a and b in Eq. (1) and M_2 and M_4 are obtained from a Taylor expansion of the first term, leading to $M_2 = a^2 + b^2/3$ and $M_4 = 3a^4 + 2a^2b^2 + b^4/5$. The result of using a function of this type to approximate the time domain NMR signals is shown in Fig. 1. One approximation shown in the figure is the best fit obtainable with a function in the form of Eq. (1). The other approximation is a superposition of two of these functions, using the calculated values of the second and fourth moments for each of the two inequivalent types of ^{1}H-atoms. The predicted time domain response using the calculated moments is in good agreement with the best fit. Differences with the experimental data are mainly due to the fact that the contribution from the amorphous part is not exponential, as was assumed for the function $G(t)$ in Eq. (1). We conclude from this that our NMR spectra agree very accurately with the prediction based on the known orthorhombic crystal stucture of PE. Looking again at the calculated values of the second and fourth moments, notice that their ratio $M_4/(M_2)^2$ is about 2.4. For a gaussian line shape this ratio is 3. This shows immediately

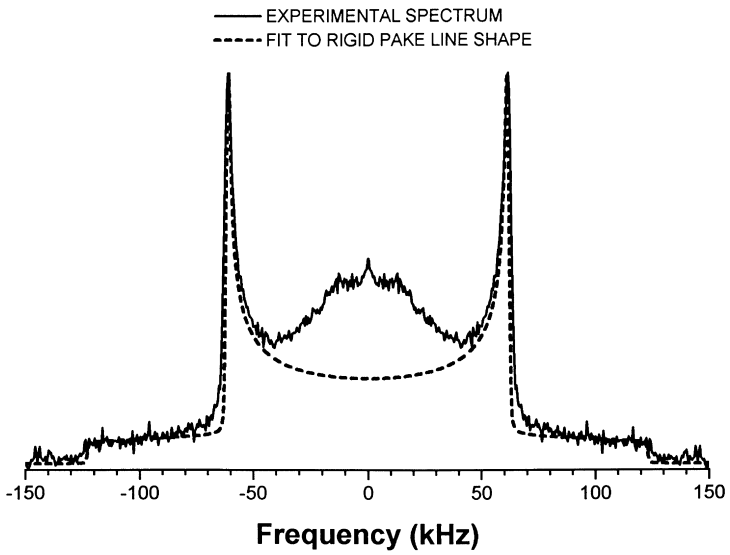

Fig. 3. The ^{2}H-NMR spectrum obtained by Fourier transformation of the response to a quadrupole-echo experiment, compared to a spectrum calculated for a powder of rigid PE crystals.

that the observed orthorhombic spectrum deviates from a gaussian line shape, as had already been noticed from the approximations with gaussian functions in Fig. 2.

2.2. Deuteron NMR spectra

Although in deuteron NMR the dipolar interactions which govern the proton line shapes are still present, they are very small compared to the dominant interactions between the electrical quadrupole moment eQ of the deuterons ($I = 1$) and the Electric Field Gradient (EFG) at the site of the deuterons. In a deuteron NMR spectrum the combined Zeeman and quadrupole Hamiltonians lead to resonance frequencies

$$\omega = \omega_0 \pm \frac{1}{2}\delta(3\cos^2\Theta - 1 + \eta\sin^2\Theta\cos 2\Phi)$$
$$= \omega_0 \pm \omega_Q(\Theta, \Phi), \qquad (2)$$

In this expression $\delta = (3/4)e^2qQ/\hbar$, while eq and η are the largest component and the asymmetry parameter of the EFG tensor, respectively; ω_0 and ω_Q represent the Zeeman frequency and the quadrupole frequency shift, respectively, and Θ and Φ are the polar angles of the external magnetic field $\vec{B}_0$ in the principle axes system of the EFG-tensor.

In PE the electric field gradient at the site of the deuterons is nearly axially symmetric along the C–D bonds, so $\eta = 0$. Therefore, for a polycrystalline sample, in which the orientations of the EFG tensor at the deuteron sites have an isotropic distribution, we expect that the quadrupole echo spectrum arising from the two transitions in Eq. (2) is the "Pake doublet", typical for a static solid.

Fig. 3 shows a ^{2}H NMR spectrum of PE at 293 K in the orthorhombic phase. This spectrum indeed consists of a Pake doublet, but it is combined with some additional intensity in the middle of the spectrum. The latter is caused by the amorphous material in the sample. Since only high temperature experiments were performed, the amorphous part is seen as the structureless line superimposed in the middle of the spectrum. On increasing the temperature, this line narrows considerably.

Hentschel et al. [13,14] measured spectra at low temperature (123 K), where they found a distance between the peaks of the Pake doublet of 123.4 kHz for completely rigid PE crystals. This corresponds to a value of the quadrupole coupling constant $e^2qQ/\hbar$ of $2\pi \times 164.5$ kHz. We used this value for the calculated spectrum shown in Fig. 3. The result fits quite well to the experimental spectrum taken at 293 K. Therefore, at room temperature the PE crystals can still be regarded as rigid.

On increasing the temperature, the shape of the observed spectrum starts to deviate from a Pake doublet towards a powder spectrum corresponding to a non-zero value of the asymmetry parameter η. This has been shown in Fig. 7 of the preceding paper [22]. This asymmetry effect was observed previously by Hentschel et al. [13]. They showed that the asymmetry can be accounted for by assuming a model where the CD_2 units in the PE chains perform oscillations about the chain axes. Since the nature of these oscillations could very well be a disorderly jump or even diffusion process with a certain average jump angle as amplitude, we prefer to speak about *reorientations* of the chain segments. The asymmetry parameter obtained by averaging the EFG tensor over two C–D-bond orientations, related by an angle 2Θ, is

$$\bar{\eta} = \frac{\overline{3\sin^2\Theta}}{\overline{3\cos^2\Theta - 1}} \qquad (3)$$

A method for the analysis of the effects of jump motion

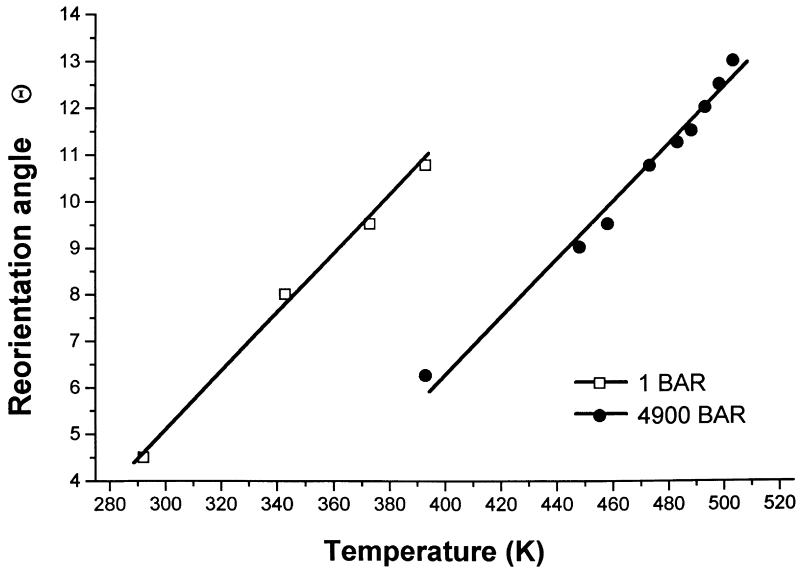

Fig. 4. Temperature dependence of the reorientation angles in orthorhombic PE at low and at high pressure.

on a quadrupole echo spectrum has been developed by Greenfield et al. [30]. It allows the calculation of the line shape resulting from the C–D-bond jumping between several orientations, as a function of the mean time between jumps. By approximating the reorientations of the chains by a model in which the C–D bonds perform a two site jump motion over an angle 2Θ, our spectra have been fitted on the basis of this method by using a computer program, kindly made available to us by the authors. The figure shows some of the observed spectra and the corresponding simulated spectra. Extremely good fits have been obtained in this way. The root mean square reorientation angles can be derived from the fits with an accuracy of one degree. The absence of broadening due to the expected presence of a distribution of reorientation angles might seem strange at first sight. This can be explained by assuming that the C–D bonds change their reorientation angle over such a distribution fast enough compared to the expected broadening. In that case only one sharply defined average reorientation angle will be visible in the spectrum.

The dependence of the root mean square value of the angle Θ on temperature is shown in Fig. 4. On increasing the temperature, Θ increases steadily from 4.5° at 292 K to 11° at 393 K at 1 bar. At 4900 bar, Θ increases from 6° at 393 K to 12.5° at 500 K. In order to determine the minimum rate of reorientation, additional simulations have been run.

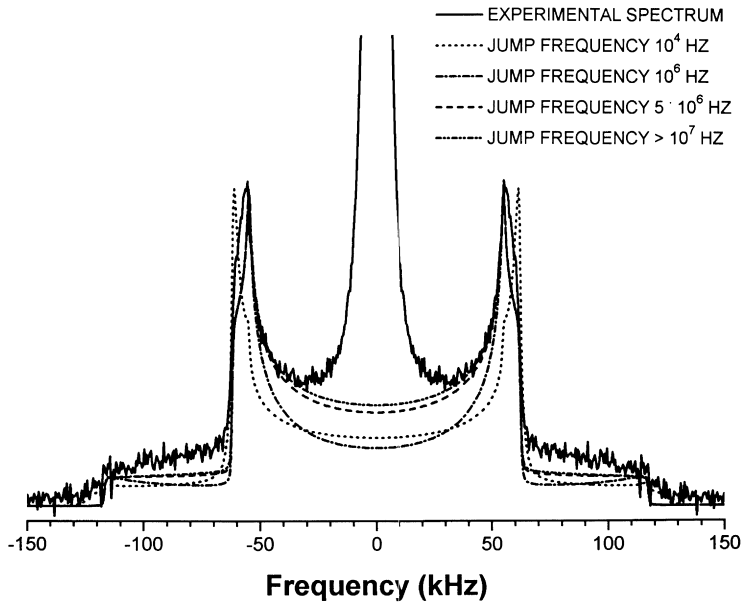

Fig. 5. Determination of the minimum reorientation rate of the chains, required for the model.

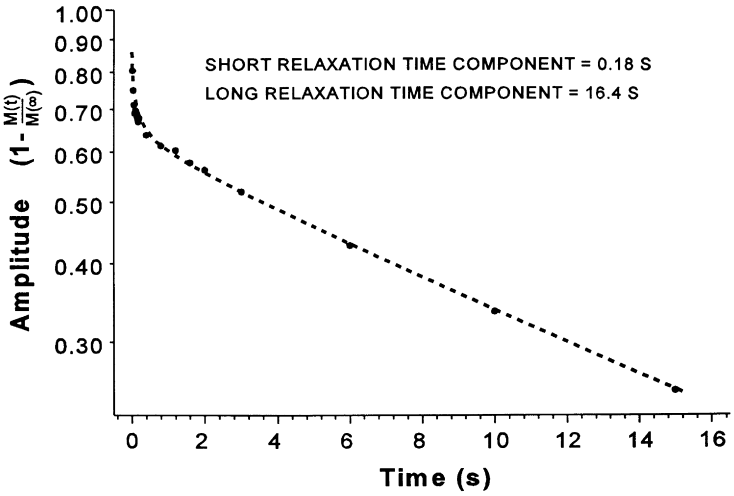

Fig. 6. Time dependence of ^{2}H-NMR echo amplitude in a typical T_1^D experiment on deuterated PE.

Some of the results are given in Fig. 5. The figure shows calculated spectra for an average amplitude angle of 11.5° compared to an experimental spectrum taken at 4900 bar and 473 K. It can be seen that the calculated spectra start to approach the experimental spectrum only if the reorientation is faster than 5×10^6 Hz. This rate is large enough to make chain reorientation a mechanism for spin–lattice relaxation.

2.3. Spin–lattice relaxation

The processes of proton spin–lattice relaxation (T_1^H) and rotating frame relaxation ($T_{1\rho}^H$) respectively) have been measured as a function of temperature at many different pressure values. The deuteron spin–lattice relaxation time T_1^D has been measured only at 1 bar and at 4900 bar. Therefore most results shown in this paper are data at 1 bar and 4900 bar in order to compare the results of different experiments. The results from experiments performed at other pressure values have been shown in the preceding paper [22].

A typical example of the behaviour of the deuteron spin–lattice relaxation in deuterated PE is shown in Fig. 6. The relaxation curve shows at least two components: one, caused by the mobile amorphous part of the sample and another component due to the crystalline material. Because of their frequency shifts, caused by quadrupole coupling, spin diffusion between the deuterons within and between both parts is only very slow. We have obtained the time constants for both parts by fitting the sum of two exponentials to the relaxation curve.

The dependence of T_1^D on the frequency in the spectra has also been determined, allowing verification of the attribution of the relaxation curve components to the amorphous and crystalline parts of the sample. In this way we have verified that the fast decaying component of the deuteron spin–lattice relaxation is due to the amorphous part and that the component with the longer T_1^D is caused by the crystalline part of the sample.

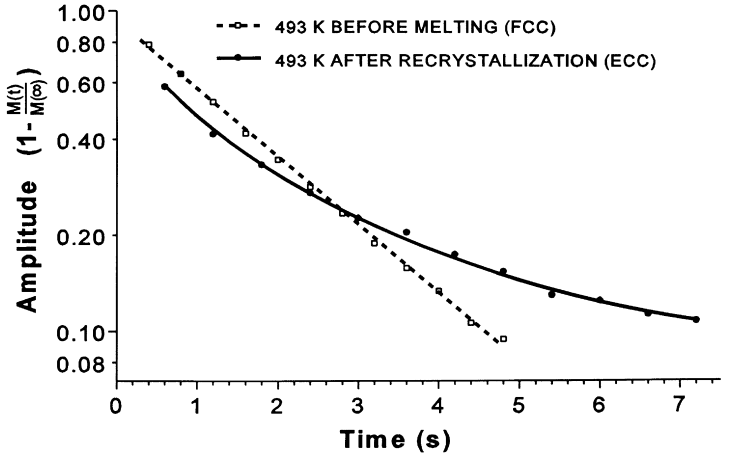

Fig. 7. T_1^H relaxation behaviour (at 4900 bar) before and after high pressure crystallization.

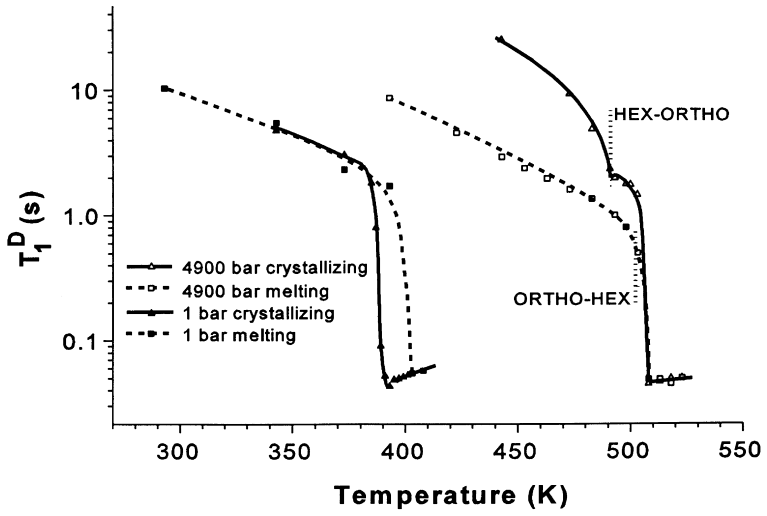

Fig. 8. Temperature dependence of the long T_1^D components at 1 bar and at 4900 bar.

The T_1^H relaxation curves are practically single exponentials in which separate long and short components cannot be distinguished although the relaxation times are expected to be different for the crystalline and non-crystalline parts. Presumably, the magnetization in the different parts of the sample is strongly coupled by spin diffusion. Evidence supporting this interpretation has been obtained from experiments performed after crystallization at high pressure. As has been discussed in the preceding paper [22], it appears that after crystallization in the hexagonal phase PE acquires the ECC structure while the crystallinity becomes much higher. The T_1^H experiments on such crystals result in a typical relaxation curve that is clearly not a single exponential, as can be seen in Fig. 7. When the crystalline parts become very large and well defined as is believed to be the case for the extended chain crystals obtained after high pressure crystallization, the coupling of the different areas by spin diffusion is no longer strong enough to let *all* magnetization decay with one overall relaxation time constant. Some of the longer relaxation times expected for the crystalline parts then become visible. These longer relaxation times also appear in Fig. 5 (middle) of Ref. [22], showing the overall T_1^H values as a function of temperature. These values have been obtained at a constant pressure of 4900 bar by taking an untreated sample of PE (Hostalen GUR 403) in which the crystalline part has a folded chain orthorhombic structure, first through the transition to the hexagonal phase and then to the liquid phase. Subsequently, the temperature is lowered and the sample first transforms into the hexagonal phase and then back in the orthorhombic phase but now with an extended chain morphology. The dramatic increase in relaxation times there clearly shows the increased crystallinity after high pressure crystallization.

In our experiments also the $T_{1\rho}^H$ relaxation curves are very close to single exponentials, so different components originating from the crystalline and non-crystalline fractions cannot be distinguished. Probably, because of the high crystallinity of the material, the components with short relaxation times expected from the non-crystalline fractions are too small to give an observable contribution to the signal. The untreated (FCC) material has a crystallinity of about 80%, while the crystallinity of the ECC material obtained after high pressure crystallization was roughly estimated from echo experiments at ambient pressure to be about 90%. However, even if the expected amplitude of non-crystalline contributions would just be large enough to be observable, spin diffusion between the protons is presumably strong enough to make the relaxation process appear exponential. The dependence of the $T_{1\rho}^H$ behaviour on the crystallinity of the sample is clearly visible in Fig. 5 (bottom) of Ref. [22]. The figure shows that the $T_{1\rho}^H$ measured in the highly crystalline ECC material is about a factor two larger than in the untreated material, which contains a larger amorphous fraction. We note that very slow components cannot be observed in our experiments, since spin-locking times are limited to about 150 ms in this study.

2.4. Proton spin–lattice relaxation times

T_1^H is sensitive to motions of the hydrogen atoms having frequencies of the order of the Zeeman frequency, which in our experiments is 180 MHz. The temperature dependence of T_1^H shows that over a large temperature range in the orthorhombic phase the mechanism behind the proton spin–lattice relaxation is in the extreme narrowing limit. As will be seen from T_1^D and $T_{1\rho}^H$ experiments in the following, the angular reorientational motion of the CH_2-groups present in the orthorhombic crystals occurs at a rate of the order of 1 MHz. These reorientations are neither fast nor large enough to be the mechanism for proton spin–lattice relaxation. The same can be said for other kinds of motion like chain diffusion. Therefore the measured values of T_1^H

are probably governed by spin diffusion to and relaxation in the amorphous and interfacial fractions and at mobile centers in the sample, like end groups and crystal defects.

As will be discussed in the next paper [31], the reorientational motion of the CH_2-groups becomes less restricted in the hexagonal phase. On increasing the temperature, the reorientation angles increase and the motion gradually becomes quasi-isotropic, while the reorientation rate increases rapidly. This is what causes the rapid decrease of T_1^H near the phase transition.

Since crystallinity and conformational disorder change as a function of temperature and pressure, T_1^H is a very good probe for the investigation of phase transitions in PE.

2.5. Relaxation times T_1^D and $T_{1\rho}^H$

The spin–lattice relaxation of the deuterons in the crystalline part of the sample is caused by the reorientational motion of the chain segments, observed in the ^{2}H NMR spectra in Fig. 7 of the preceding paper [22]. Because of the limited reorientation angles, it is not a very effective process. As can be seen in Fig. 8, T_1^D in the orthorhombic phase is on the low temperature branch of the deuteron relaxation temperature dependence, far from its minimum, therefore the characteristic frequencies of this motion are lower than the deuteron Zeeman frequency $\omega_D = \gamma_D B_0 = 2\pi \times 27.3 \times 10^6$ Hz.

Since the details of the reorientational motion observed in the ^{2}H spectra are not known, we cannot derive a quantitative expression for the spin–lattice rate caused by it. An approximation can be obtained by regarding the motion as a jump process over a single angle 2Θ between two orientations of the C–D bonds, while the mean time between jumps is τ. One may then use the expression (32) and Table 2 from the analysis by Torchia and Szabo [32] to derive a powder averaged value of the deuteron spin–lattice relaxation rate:

$$\frac{1}{T_1^D} = \frac{9}{80}\left(\frac{e^2qQ}{\hbar}\right)^2 \sin^2 2\Theta \frac{1}{\omega_D^2\tau} \tag{4}$$

This expression is obtained in the slow motion regime $\omega_D\tau > 1$. (We note that the difference with the familiar result obtained for isotropic reorientation in Ref. [28; Eq. (VIII-138)] is the reduction factor $R = (3/4)\sin^2 2\Theta$).

From this simplified model, giving T_1^D as a function of the mean time between jumps and the reorientation angle, we can check the interpretation of our measurements in terms of reorientations of CH_2-units about the chain axes. We start with the experiments at 4900 bar. As shown in Fig. 8, the value of T_1^D measured at 443 K is 2.6 s. This temperature is chosen because it is the temperature where $T_{1\rho}^H$ shows a minimum during heating (see Ref. [22; bottom of Fig. 5]). Assuming the same motional process to be responsible for both $T_{1\rho}^H$ and T_1^D, the correlation time τ should be $(4\pi\nu_1)^{-1} = 8 \times 10^{-7}$ s. Using this in Eq. (4) gives $\Theta = 7.9°$. From Fig. 4 it can be seen that at the same values of temperature and pressure from the ^{2}H spectra we obtain $\Theta = 8.75°$. Both values agree nicely. At ambient pressure the $T_{1\rho}^H$ minimum has been found to occur around 303 K. The T_1^D value is about 7 s in this case. The use of these values in the same calculation gives a reorientation angle of 4.75°, which is in agreement with the 5° angle from the ^{2}H NMR spectra.

The relaxation times $T_{1\rho}^H$ are sensitive to molecular motions having frequencies of the order of ν_1, corresponding to the spin-locking field B_1. This frequency is of the same order as was found from the ^{2}H NMR spectra for the rate of the reorientation of the CH_2-groups in the crystalline part of the sample. It is expected therefore that the reorientational motion of the chain segments is also the mechanism for $T_{1\rho}^H$ in the crystalline component.

An approximation for calculating $T_{1\rho}^H$ in the two-site jump model can be found by looking closely at the dipolar coupling of hydrogens on the same CH_2 group. The dipolar coupling between two such hydrogens gives the most important contribution to the $T_{1\rho}^H$-mechanism. Under the same reorientations of the chain this coupling transforms in the same way as the quadrupolar coupling in the C–D bond. Using this similarity of both couplings it follows from the expression [33,34] for $T_{1\rho}^H$, valid for isotropic motion, that in the two-site jump model

$$\frac{1}{T_{1\rho}^H} = \frac{3}{10}\left(\frac{\gamma^4\hbar^2 f^2}{r_{12}^6}\right) \times \frac{3}{4}\sin^2 2\Theta\left[\frac{3\tau/2}{1+4\omega_1^2\tau^2}\right]. \tag{5}$$

In this expression the terms containing $\omega_0 = \gamma_H B_0$ in the original expression have been neglected because this expression will now be applied in the vicinity of the $T_{1\rho}^H$ minimum, where $\omega_1\tau = (1/2)$ and $\omega_0\tau \gg 1$. The factor $(3/4)\sin^2 2\Theta$ is the same reduction factor as the one that has been determined earlier from the expression (4) for T_1^D. According to the experimental results (in Ref. [22; bottom of Fig. 5]) obtained at 4900 bar before melting the sample, a $T_{1\rho}^H$ minimum of 4.8 ms occurs at about 445 K, while after crystallization a minimum of 9 ms occurs at about 423 K. When values of Θ, obtained from T_1^D of the crystalline component are used in Eq. (5), the resulting values of $(T_{1\rho}^H)_{min}$ are 3.6 ms and 5.5 ms, respectively. These values are in reasonable agreement with the measured values.

This analysis clearly shows that the process of small-angle reorientation of the CH_2-groups is the main mechanism for proton-spin rotating frame relaxation in the crystalline fraction, resulting in a minimum value of $T_{1\rho}^H$ of the order of 5 ms. As has been mentioned above, $T_{1\rho}^H$ in the ECC material is always longer than in the untreated material. Presumably, this is caused by the more rapid relaxation due to more isotropic CH_2-reorientation in the amorphous fraction which, in our experiments, cannot be distinguished from the relaxation in the crystalline fraction. From its minimum value $T_{1\rho}^H$ increases with increasing temperature, due to the increasing rate of small-angle reorientation of the CH_2 groups. As may be seen in the bottom of Fig. 5 of the preceding paper [22], in the ECC material $T_{1\rho}^H$ shows a maximum just below the orthorhombic–hexagonal phase

transition. As will be further discussed in the next paper [31], the increased rate of relaxation just below the transition is due to longitudinal chain diffusion. In the untreated material (see also Fig. 3 of the preceding paper [22]) this effect is masked by the larger contribution of the faster relaxation in the amorphous fraction.

We note here that the simplification of the process of reorientation of the chain segments to a two-site jump model is rather crude. Presumably, this motion is much more diffusive in nature, leading to a complicated frequency spectrum. Large angle reorientations will occur on a longer time scale than small angle variations. The observed approximate consistency of the values of T_1^D, $T_{1\rho}^H$ and Θ is only valid for those values of the mean time τ between jumps that are larger than about 10^{-7} s. It breaks down at higher temperature.

3. Conclusions

At ambient pressure the orthorhombic crystalline form of PE is a rigid molecular solid, from low temperature up to the region close to the melting transition. The proton NMR line shape at room temperature is in excellent agreement with the prediction based on the rigid structure known from X-ray data. Apart from some high-frequency mobility at end groups and other lattice defects, as observed in the measurement of the proton spin–lattice relaxation rate, only small-angle reorientational motion of the the CH_2 groups is observed on the time scale of the deuteron NMR line shape and relaxation rate measurements and of the proton $T_{1\rho}^H$ data. Most of these facts were already known. Our results have provided more accurate information, especially on the characteristics of the reorientational motion. We found the reorientation angle to increase from 4.5° at room temperature to 11° at 393 K (about 10 K below the phase transition). In a similar study performed in this region at ambient pressure, Hentschel et al. [13] found the angle to increase from 5° at room temperature to 12° at 383 K. These values agree very well with our results. We found the characteristic time of the motion to be between 10^{-7} and 10^{-6} s.

The most important new contribution is the extension of the above information to high pressure. At high pressure PE was found to show similar behaviour. However, the application of pressure results in a considerable reduction of the amplitude of the reorientational motion of the CH_2 groups. At 4900 bar the reorientation amplitude angle increases from 6° at 393 K to 12.5° at a temperature of 500 K. An other important observation in this study is the spectacular increase of the degree of crystallinity of PE by solidification through the hexagonal phase.

References

[1] Newman R. J Chem Phys 1950;18:1303.
[2] Rempel RC, Weaver HE, Miller RL. J Appl Phys 1957;28(10):1082.
[3] Kitamaru R, Horii F. Adv Polym Sci 1978;26:139.
[4] Edzes HT, Bernards JPC. J Am Chem Soc 1984;106:1515.
[5] VanderHart DL, Khoury F. Polymer 1984;25:1589.
[6] Schmidt-Rohr K, Spiess HW. Macromolecules 1991;24:5288.
[7] Punkkinen M, Ingman LP. Phys Stat Sol 1978;46:213.
[8] Rosenke K, Sillescu H, Spiess HW. Polymer 1980;21:757.
[9] Opella SJ, Waugh JS. J Chem Phys 1977;66(11):4919.
[10] Hentschel D, Sillescu H, Spiess HW. Macromolecules 1981;14:1605.
[11] Bridges BJ, Charlesby A, Folland R. Proc R Soc Lond 1979;A367:343.
[12] Alamo RG, Viers BD, Mandelkern L. Macromolecules 1995;28:3205.
[13] Hentschel D, Sillescu H, Spiess HW. Makromol Chem 1979;180:241.
[14] Hentschel D, Sillescu H, Spiess HW. Polymer 1984;25:1078.
[15] Kulik AS, Prins KO. Polymer 1994;35(11):2307.
[16] Odajima A, Sauer JA, Woodward AE. J Phys Chem 1962;66:718.
[17] Kitamaru R, Horii F, Zhu Q, Bassett DC, Olley RH. Polymer 1994;35(6):1171.
[18] Havens JR, VanderHart DL. J Magn Res 1985;61:389.
[19] Tzou DL, Schmidt-Rohr K, Spiess HW. Polymer 1994;35(22):4728.
[20] McBrierty VJ, McDonald IR. Polymer 1975;16:125.
[21] de Langen M, Prins KO. Rev Sci Instrum 1995;66:5218.
[22] de Langen M, Prins KO. Polymer, 2000;41:1175.
[23] Spiess HW, Sillescu H. J Magn Res 1981;42:381.
[24] Davis JH, Jeffrey KR, Bloom M, Valic MI, Higgs TP. Chem Phys Lett 1976;42:390.
[25] Levitt MH. J Magn Res 1982;48:234.
[26] Levitt MH, Suter D, Ernst RR. J Chem Phys 1984;80:3064.
[27] Rhim WK, Pines A, Waugh JS. Phys Rev B 1971;3:684.
[28] Abragam A. The principles of nuclear magnetism. Oxford: Oxford University Press, 1961.
[29] Bassett DC, Block S, Piermarini GJ. J Appl Phys 1974;45(10):4146.
[30] Greenfield MS, Ronemus AD, Vold RL, Vold R. J Magn Res 1987;72:89.
[31] de Langen M, Luigjes H, Prins KO. Polymer 2000;41:1193.
[32] Torchia DA, Szabo A. J Magn Res 1982;49:107.
[33] Look DC, Lowe IJ. J Chem Phys 1966;44:2995.
[34] Mehring M. High resolution NMR spectroscopy in solids. Berlin: Springer, 1976.